

Liverpool Preprint: LTH 331
 hep-lat/yymmppp
 April 5th 1994

Instanton size distribution in $O(3)$

C. Michael and P.S. Spencer

DAMTP, University of Liverpool, Liverpool L69 3BX, UK

Abstract

We present calculations of the size distribution of instantons in the $2d$ $O(3)$ non-linear σ model, and briefly discuss the effects cooling has upon the configurations and the topological objects.

1 Introduction

The $O(3)$ non-linear σ -model in $(1 + 1)$ space-time dimensions has been much studied because of the properties it shares with 4-dimensional non-Abelian gauge theories: it is asymptotically free, becomes non-perturbative in the infra-red regime and has a non-trivial topology due to the homotopy class $\pi_2(S_2) = \mathbb{Z}$ of windings from $S_2 \rightarrow S_2$.

It has been known for some time that the standard lattice discretisation of the $O(3)$ model has problems—for example, the lattice topological susceptibility does not obey naïve scaling laws. Lüscher has shown [1] that this is due to the model being dominated by short-range fluctuations. Formulating this theory on the lattice implies a minimum size to these fluctuations, and so the important contributions from fluctuations smaller than one lattice spacing are absent. There is also the problem that additional short-range fluctuations (known as lattice artefacts) are present in the lattice formulation and not in the continuum. These are unphysical field configurations such as the winding of the field around one plaquette, giving rise to spurious contributions to the topological charge [1].

The model is well understood in some respects—for instance an exact expression for the mass gap is known [2]. It is thus a natural candidate for a theory which one can attempt to understand in terms of the vacuum structure. In this paper we explore the nature of the vacuum via numerical simulation in Euclidean time. We concentrate on large scale structures in the vacuum - such as those arising from instantons. In order to focus on such extended features in the vacuum, we use a procedure to smooth out local fluctuations. A cooling algorithm is used

to achieve this. The basic idea is that a local smoothing of the fields should preserve long range features such as instantons. In [3] we explored this by varying the details of the cooling procedure and presenting qualitative features of the resulting topological charge distribution.

In this work we wish to make a quantitative study of the nature of the topological distribution in the vacuum. Such a cooling procedure will modify the short distance properties of the vacuum, so we explore the distribution of the size of topological objects since we can expect that the large size objects are unchanged under cooling. By varying the lattice spacing and the extent of cooling, we are able to present results for the physical distribution of large scale topological fluctuations.

2 The $O(3)$ Model on a Lattice

The continuum $2d$ $O(3)$ Euclidean action S_E is defined as:

$$S_E = \frac{1}{2g^2} \int d^2x (\partial_\mu \phi)^2 \quad (1)$$

with ϕ an $O(3)$ vector and the constraint $\phi^2 = 1$.

Much use has been made of so-called “improved” actions in $O(3)$ (eg [4, 5]) and more recently “over-improved” [6] and “perfect” [7] lattice actions have been proposed; here we use the more local nearest-neighbour action. This is appropriate since we wish to develop techniques that will extend to other theories (such as 4-dimensional $SU(N)$) where a perfect lattice action is not yet available. Taking the discrete form of the derivative (μ running over the space-time directions):

$$\partial_\mu \phi(x) \rightarrow \Delta_\mu \phi_x = \frac{1}{a} (\phi_{x+\mu} - \phi_x) \quad (2)$$

where ϕ_x is now a field associated with the site x and a is the lattice spacing (hereafter set to 1), the lattice action is:

$$\begin{aligned} S_L &= \frac{1}{2g^2} \sum_{x,\mu} (\phi_{x+\mu} - \phi_x)^2 \\ &= \frac{1}{g^2} \sum_x (2 - \phi_F(x) \cdot \phi_x) \end{aligned} \quad (3)$$

with the index μ again running over directions on the lattice, and ϕ_F defined as the sum over nearest neighbours:

$$\phi_F(x) = \sum_\mu \phi_{x\pm\mu}. \quad (4)$$

The continuum topological charge Q is defined as:

$$Q_f^T = \frac{1}{8\pi} \int d^2x \epsilon_{\mu\nu} \epsilon_{ijk} \phi_i \partial_\mu \phi_j \partial_\nu \phi_k \quad (5)$$

and is by definition an integer. However, if this “field theoretical” definition is placed naïvely onto the lattice, it returns non-integer values and acquires a renormalisation factor [4,8]. There are other “geometric” lattice definitions that return integers, one example being given in [1,9,10], based on the mapping $S_2 \rightarrow S_2$, by calculating the signed area of the spherical triangles formed by the ϕ fields around a plaquette. The contribution to the total charge from a site x^* on the dual lattice is given by:

$$Q_g^T(x^*) = \frac{1}{4\pi}((\sigma A)(\phi_1, \phi_2, \phi_3) + (\sigma A)(\phi_3, \phi_4, \phi_1)) \quad (6)$$

where

$$\sigma(\phi_1, \phi_2, \phi_3) = \text{sign}(\phi_1 \cdot \phi_2 \times \phi_3) \quad (7)$$

and $A(\phi_1, \phi_2, \phi_3)$ is the area of the spherical triangle on the unit sphere mapped out by the ϕ fields, and the subscripts 1, 2, 3, 4 refer to the corners of a plaquette labelled anti-clockwise. Clearly there are two ways to triangulate a plaquette and the difference in the contribution to Q^T from the two triangulations is 0 for configurations with small action, but can be ± 1 for other field configurations.

There are arguments against the use of such a charge definition, particularly in calculations of the topological susceptibility, χ_t , in CP^{N-1} theories with small values of N . Campostrini et al have shown [11] that for values of $N = 10$ and larger, the geometrical formulation gives a sensible definition of χ_t , but not for lower values of N .

3 Instantons in $O(3)$

Since we shall wish to compare fluctuations in the topological charge density with instantons, we now discuss the details of the instanton contributions. Let us first summarise the results for the continuum in an infinite space-time region.

With ϕ written in terms of the projective fields $\omega, \bar{\omega}$:

$$\phi_1 = \frac{\omega + \bar{\omega}}{\omega\bar{\omega} + 1}, \quad \phi_2 = \frac{\omega - \bar{\omega}}{i(\omega\bar{\omega} + 1)}, \quad \phi_3 = \frac{\omega\bar{\omega} - 1}{\omega\bar{\omega} + 1} \quad (8)$$

(1–3 here are $O(3)$ indices) a field configuration *representing* a single (continuum) instanton of size $|\rho|$ at position r can be explicitly constructed via [9,10,12,13,14]

$$\omega = \frac{\rho}{z - r} \quad (9)$$

with $z = x + it$ the coordinate in the complex plane. This can be easily extended to generate multiple instanton configurations; an N -instanton configuration has the form:

$$\omega = \sum_{i=1}^N \frac{\rho_i}{z - r_i} \quad (10)$$

and has topological charge N . Similarly, a multi-anti-instanton configuration with $Q^T = -N$ can be generated via [13, 14]:

$$\omega = \sum_{i=1}^N \frac{\bar{\rho}_i}{\bar{z} - \bar{r}_i} \quad (11)$$

It should be noted that a configuration containing both instantons and anti-instantons is not strictly a solution of the classical equations of motion. In [14], Bukhlostov and Lipatov construct a general configuration containing N^I instantons and N^A anti-instantons via

$$\omega = \left(\sum_{i=1}^{N^I} \frac{\rho_i^I}{z - r_i^I} \right) \left(\sum_{j=1}^{N^A} \frac{\bar{\rho}_j^A}{\bar{z} - \bar{r}_j^A} \right) \quad (12)$$

based on the assumption that the (anti-)instantons have sizes small compared to their separations, $\rho_i^I, \rho_j^A \ll |r_i^I - r_j^A|$, or essentially different scales, e.g. $\rho_i^I \ll \rho_j^A$, i.e. on the assumption that the instantons and anti-instantons are weakly interacting. In this scenario, the $O(3)$ model becomes equivalent to an exactly soluble fermion model.

With ϕ and ω as in eqs. 8 and 9 above, the action and topological charge density become:

$$S(z), Q(z) \propto \frac{\rho^2}{(\rho^2 + |z - r|^2)^2}. \quad (13)$$

where here the size parameter ρ is an abbreviation for $|\rho|$ of eq. 9. A similar relation holds true for multi-instanton configurations. It should be noted that, for a general field configuration, the action density is positive definite, but the charge density is not, having contributions from both instantons and anti-instantons for which the charge has opposite signs. The topological charge sets a lower bound on the action [12]:

$$S \geq \frac{4\pi}{g^2} |Q| \quad (14)$$

from which it can be deduced that a single instanton configuration has action S_I :

$$S_I = \frac{4\pi}{g^2}. \quad (15)$$

Clearly an N -instanton configuration generated from eq. 10 will have an action $4\pi N/g^2$.

On a space with toroidal boundary conditions, there are *no* exact single-instanton solutions to the equations of motion. An argument for this is given in Appendix A. The simplest solution has two instantons with their ρ parameters satisfying $\rho_1 = -\rho_2$. For solutions with several instantons and anti-instantons, the constraints from the toroidal boundary conditions will be relatively less severe. On the lattice the boundary conditions are toroidal, so the one instanton configuration based on eq. 9 will be only a metastable field configuration.

Furthermore, the lattice action differs from the continuum action to order a where a is the lattice spacing. As shown in [6], this implies that instantons are not exact solutions to the lattice equations of motion. For the conventional lattice action (as used here) this results in instantons shrinking slowly under application of the equations of motion.

If a dilute gas of instantons and anti-instantons is a good approximation, it is possible to deduce the nature of their size distribution from renormalisation group arguments—see [15, 16, 13]. For the $O(3)$ model this approximation gives

$$\frac{S}{V} = e^{-4\pi/g^2} g^{-4} \int_0^\infty d\rho \frac{f(\rho M)}{\rho^3} \quad (16)$$

where the 4 powers of $1/g$ come from scale and translation considerations, and the 3 powers of $1/\rho$ in the integrand come from dimensional analysis. f is the function we wish to determine and M the cutoff mass. g^2 is dimensionless, and as the only dimensionful quantities are ρ and M , then we should replace the bare coupling g^2 by the running coupling $\bar{g}^2(\rho M)$. Renormalisation group theory implies that for any observable quantity, ρM and g should enter only in the combination

$$\frac{1}{g^2} \rightarrow \frac{1}{\bar{g}^2} = \frac{1}{g^2} - \beta_1 \ln(\rho M) + O(g^2) \quad (17)$$

with β_1 obtainable from the one-loop β -function. The form of f and hence the distribution by size can therefore be deduced. For $O(3)$, $\beta_1 = 1/2\pi$ [17], (see also [13]) and gives a factor of $\rho^2 M^2$, implying $f \propto \rho^2 M^2$ to accommodate this, and giving a distribution that goes as the reciprocal of the instanton size. This explains why it is so difficult to determine the topological charge on a lattice since the distribution is peaked at small size where the lattice modifies the behaviour substantially. However, the large size component of the distribution should be amenable to study on a lattice and that is the topic we now address.

4 Cooling and Numerical Lattice Calculations

We use lattices of size 64×64 with 1000 sweeps between configurations. Each sweep is composed of 1 heatbath and 9 over-relaxed updates of the whole lattice. The action density distribution on a lattice configuration at $g^2 = 0.8$ is shown in fig. 1. As we found previously [3], it is not feasible to derive any useful results from such configurations since they have too much short distance fluctuation. They first need to be cooled.

Cooling, being a local update algorithm, removes the short-range noise and leaves the longer-range instantons approximately alone [4]. Our lattice action has order a effects that imply [6] that an instanton-like solution has an action close to the continuum value given in eq. 15 but which is reduced slightly as the size ρ decreases. Thus cooling, which is equivalent to iteratively implementing the

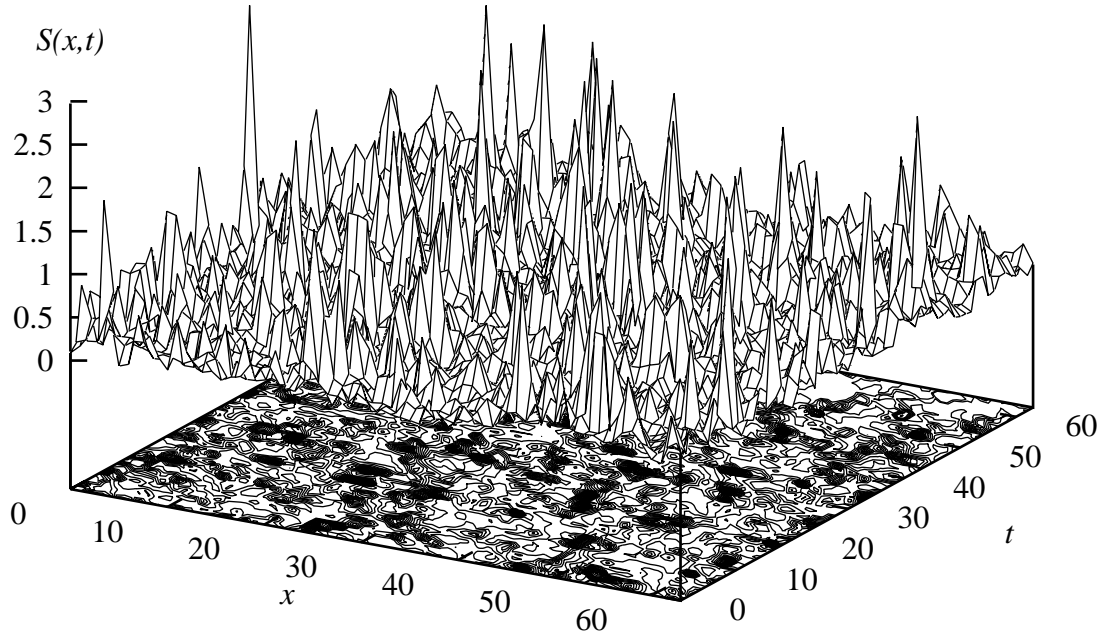


Figure 1: The action density from an uncooled configuration, generated at $g^2 = 0.8$.

equations of motions, will affect the size of an instanton. Protracted cooling on a single, moderately sized instanton gradually reduces its size to that of one lattice spacing, and then destroys it. This is familiar from the plateaux that develop in the action as a configuration is cooled. The plateaux correspond to instantons being shrunk then destroyed. The contribution to the action from an instanton is a finite amount which depends only weakly on the instanton's size, so the action will decrease by approximately $S_I = 4\pi/g^2$ each time an instanton is destroyed. In order to analyse instanton-like features after cooling, we have to calibrate the cooling process to take account of such shrinkage under cooling.

The cooling we used was an under-relaxed cooling:

$$\phi'_x = \alpha\phi_x + \phi_F(x) \quad (18)$$

properly normalised so that $(\phi'_x)^2 = 1$, with $\phi_F(x)$ defined in eq. 4. α is a parameter which determines the severity of the cooling. The effects of varying α are discussed in [3].

We wish to study the nature of the topological charge distribution, in particular the frequency of occurrence of large objects. We assume that large scale objects will have a shape similar to that of an idealised instanton. This is based on the expectation that meta-stable solutions to the classical equations of motion will dominate the quantum vacuum, so our strategy is to analyse the topography of the cooled vacuum distribution to report on its nature.

If the action after cooling is S , then we expect to have of order $N = S/S_I$ topological objects present. The topological charge distribution $Q_g^T(x, t)$ can have either sign and so contains more information in principle than the action density $S(x, t)$. Since, however, $|Q^T(x, t)|$ closely tracks $S(x, t)$ after cooling [3]—see fig. 2—it is sufficient to use S alone. This has two advantages: it is easier to calculate numerically (particularly in more complex theories than $O(3)$) and it enables us to select regions in a way unbiased by sign so that any correlation between the distribution of instantons and anti-instantons can be studied. A further advantage is that from $S(x, t)$ it is relatively easy to devise a robust algorithm that finds N connected space-time regions.

For each cooled configuration, we select N connected regions such that each region contains an internal local maximum of the action density and is composed of all connected sites with an action density greater than half that maximum. The regions are mutually exclusive and we select them in order of decreasing value of their maximum action density. The square root of the area of each such region was then taken to parametrise the actual “size” ρ of the region.

In order to calibrate this algorithm, we first analysed artificial configurations created with one instanton generated by eqs. 8 and 9. A linear relation was found between our calculated size and the input size. Returning now to real configurations, we looked at the relation between the value of the action density at the local maximum and the size assigned to it, as eq. 13 implies, for isolated continuum instantons:

$$S(x_{max}) = \frac{4}{g^2 \rho^2} . \quad (19)$$

We compared the data from our configurations with this predicted continuum behaviour; the result is shown in fig. 3. While it is clear that our data do *not* have the exact inverse-square behaviour, it is nonetheless encouraging to see that the data lie near to the curve. Indeed, any dissimilarity between the curve and the data can be seen as further evidence that the dilute instanton gas is not the correct model for the vacuum.

Since cooling tends to shrink instantons, it is important to calibrate the amount of cooling used and the extent of this effect. This is particularly important since we wish to decrease the lattice spacing and obtain results for the continuum limit. Our cooling algorithm is local (ie. on the scale of 1 lattice spacing) and so will need to be adjusted to have the same physical effect as the lattice spacing is reduced. We would hope that cooling can be arranged to have the same effect in physical distance units. This may not be possible because though the cooling may be adjusted to have similar effects at a given short distance (in physical units), it may give different effects at a larger distance as the lattice spacing is varied.

In order to minimise such problems, we specify the cooling in terms of its effect on an instanton. Thus we cool until an isolated instanton of a given physical size is removed (ie shrunk to zero). Indeed in [3], we determined the amount of

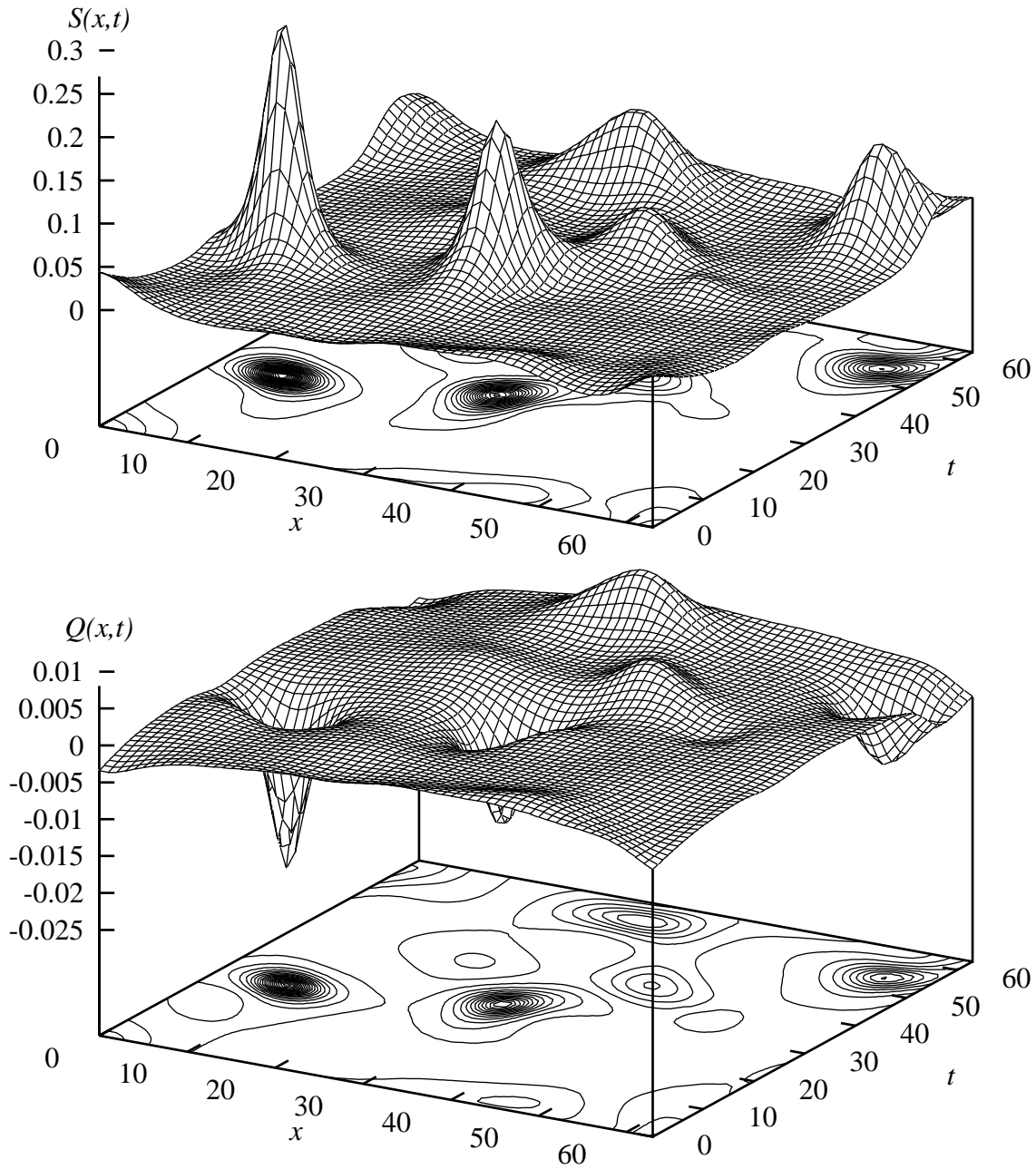


Figure 2: A cooled configuration at $g^2 = 0.8$ after 90 cooling sweeps with $\alpha = 2$.

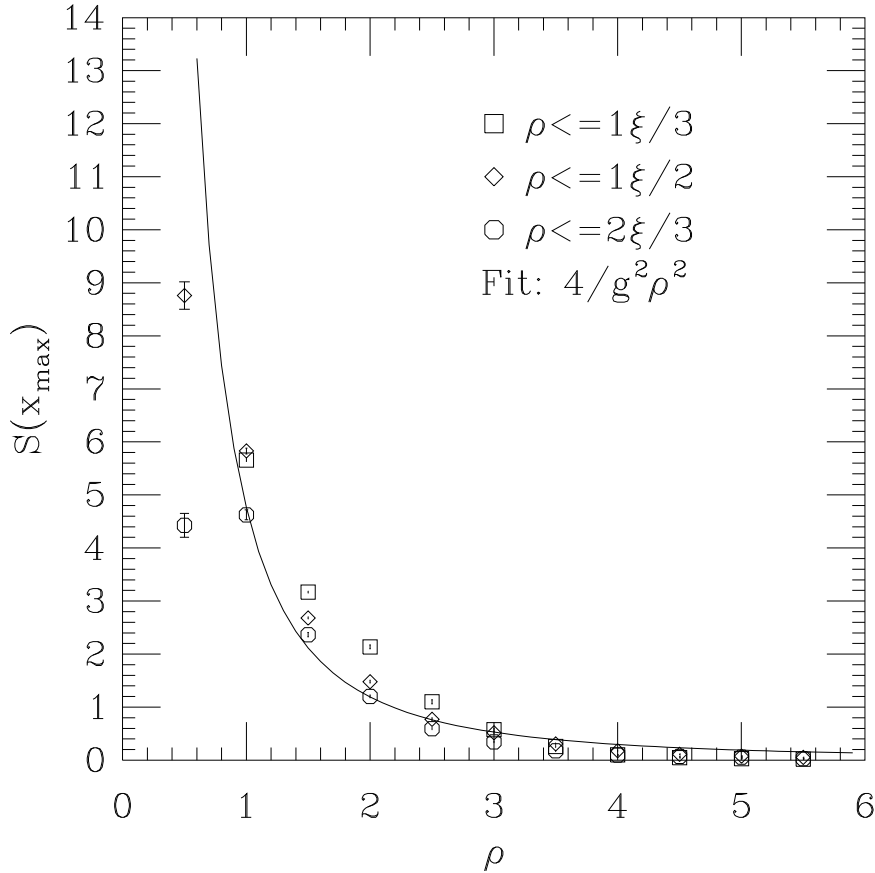


Figure 3: The relation between the value of the action density at a local maximum and the instanton ‘size’ we associated with it. For these data $g^2 = 0.84$. The curve comes from eq. 19.

cooling to use by computing the number of steps required, at a given α , to remove a single instanton of a given size generated via eq. 9. Here we specify the instanton size in physical units, i.e. in units of the correlation length ξ . We considered the cooling required to remove such instantons of size one third, one half and two thirds the correlation length, and the results are given in table 1.

Our aim is to derive a distribution of the size of topological fluctuations which is independent of both the lattice spacing (ie coupling g^2) and the cooling algorithm. We expect a weak signal from objects with large physical sizes, because of the effects of the finite lattice size and because a large instanton has small maximum action density and so may be swamped by the larger signal from smaller objects; while at small scales we expect unphysical contributions from lattice artefacts and from the size cutoff of the lattice to adversely affect the results. It was our hope that there would be some intermediate region where sensible results could be obtained.

We analyse 1000 configurations at each value of g^2 . These correspond to a

g^2	m_{eff}	L	$\rho = \xi/3$	$\rho = \xi/2$	$\rho = 2\xi/3$
0.8	0.261(1)	64	28	79	220
0.84	0.318(1)	64	17	45	106
1.00	0.551(1)	64	5	13	24

Table 1: The measured mass gap and lattice sizes at the three values of g^2 we used, and the number of cooling sweeps required, at $\alpha = 2$ to remove an instanton of size $\rho = \xi/3, \xi/2, 2\xi/3$ at each value of g^2 .

range of correlation lengths of a factor of 2, allowing us to study scaling (ie independence of the results on the lattice spacing). We checked that there was no statistically significant evidence for any auto-correlation between these configurations so that they can be treated as statistically independent in error analyses. Each configuration was cooled by the amounts shown in table 1. This range of cooling was restricted by the requirement that the instanton removed for calibration should not be too small (thus at $g^2 = 1.00$ objects of size $\rho \sim \xi/3$ correspond to less than 1 lattice spacing). At the other cooling extreme, we found that severe cooling to remove all objects of size $\rho \sim 2\xi/3$ made a rather large change to the original configuration and so tended to modify more any physics that might be present in the uncooled configuration. Consequently we took this to be the upper bound on any useful degree of cooling.

The consistency of our cooling scheme can be judged by measuring the ratio of the number $N = S/S_I$ of topological objects to the physical volume V . This should be independent of g^2 at fixed cooling level. Table 2 shows an approximate independence. This provides an estimate of the systematic error from a cooling scheme. We also see a decrease of N with increased cooling at fixed g^2 , but this is entirely to be expected.

g^2	$\rho = \xi/3$	$\rho = \xi/2$	$\rho = 2\xi/3$
0.8	0.04897(20)	0.02745(17)	0.01574(14)
0.84	0.04945(15)	0.02749(12)	0.01703(11)
1.00	0.048889(78)	0.024663(57)	0.016261(49)

Table 2: The number of objects per unit physical volume per configuration, $S/V S_I$, at the different values of g^2 under differing amounts of cooling.

We now present our results for the size distribution of topological objects found by the algorithm introduced above. In figs. 4 and 5, we have plotted $dN/V d\rho$ where both ρ and V are in units of the correlation length (as are all lengths we quote), and $N = S/S_I$.

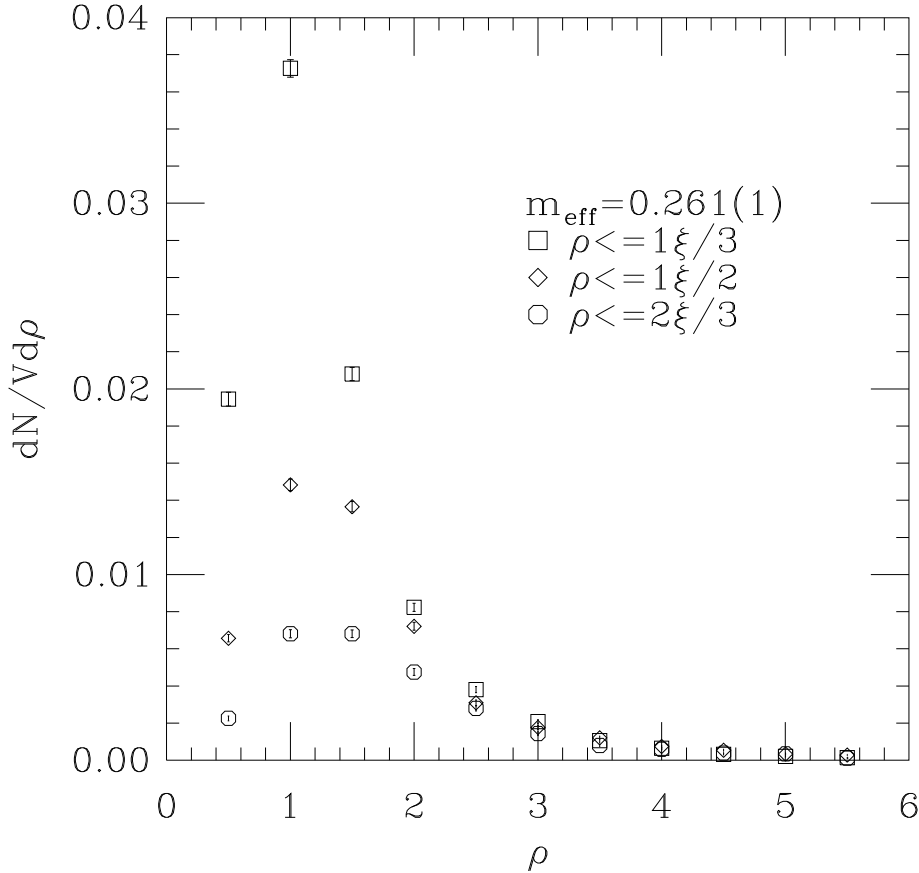


Figure 4: Size distribution data obtained from cooling the same 1000 configurations by three different amounts, the details given in table 1. For these data $g^2 = 0.8$. ρ is given in units of ξ .

Let us first discuss the effect of varying the amount of cooling at a fixed lattice spacing. We expect that objects of progressively larger sizes are modified as the cooling is increased. One would hope to see that the signal from large size objects is independent of cooling. Fig. 4 shows the data obtained from cooling the same 1000 configurations, generated at $g^2 = 0.8$, by three different amounts: to remove objects of size $\rho \sim \xi/3, \xi/2, 2\xi/3$ and smaller. As we expected, we see smaller objects progressively removed but there is a clear signal that is cooling-independent in the range $2.5 \lesssim \rho \lesssim 4.5$. For very large objects there is virtually no signal. We performed the same cooling on configurations generated at other values of g^2 and found similar signals.

We also wish to study the independence of the size distribution for changing lattice spacing when the cooling is held the same. Fig. 5 shows the data obtained at each of the values of g^2 we used, here cooled to remove objects of size $\rho \sim \xi/2$ and smaller. There is a good agreement across the range of g^2 we used in the range $3 \lesssim \rho \lesssim 5.5$; this coupling-independence is good evidence for a continuum

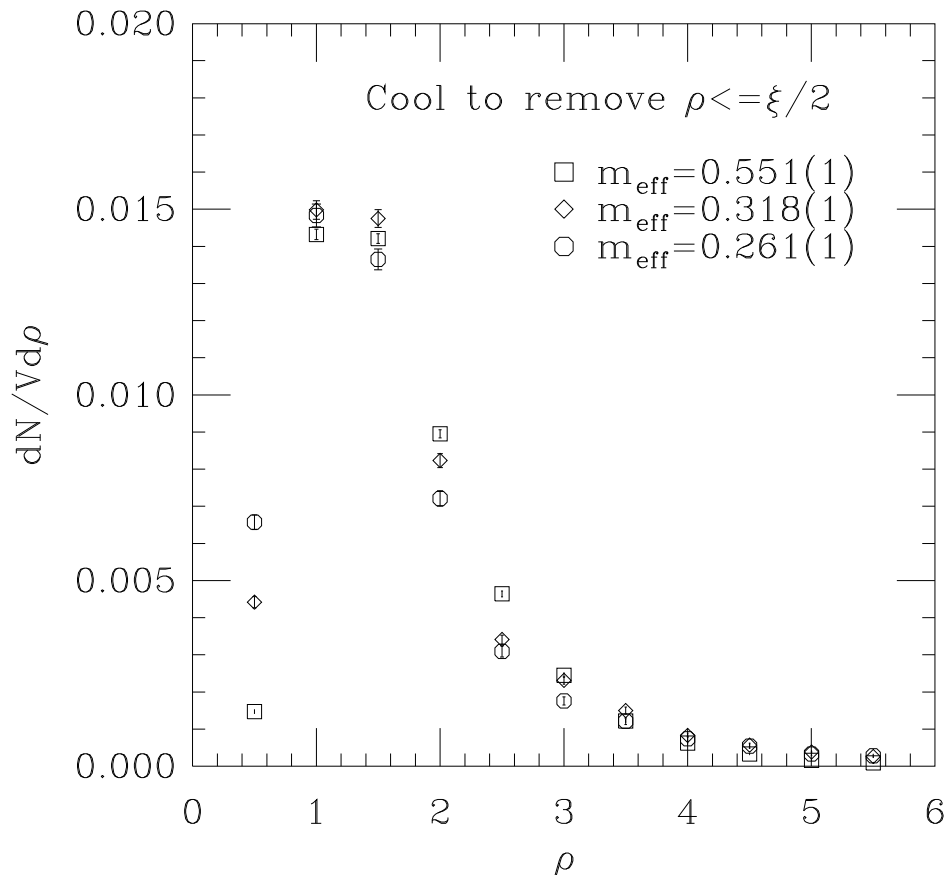


Figure 5: Size distribution data obtained from performing the same cooling on configurations generated at three different couplings, the details given in table 1. For these data, the cooling was to remove objects of size $\rho \lesssim \xi/2$. ρ is given in units of ξ .

distribution similar to that shown. For the lesser amount of cooling, we found good agreement between the results at $g^2 = 0.8$ and $g^2 = 0.84$ in a larger range, but not between these data and those calculated at $g^2 = 1.00$, where the cooling corresponded to removing objects of size less than one lattice spacing. At the greater cooling level, the agreement was significantly less than for the data shown. We would therefore propose that these are the outside limits on what useful cooling can be done without adversely affecting the physics.

In an attempt to discover something about instanton–anti-instanton interactions, we looked at the separations of objects, ie of instanton–instanton, anti-instanton–anti-instanton and instanton–anti-instanton pairs. In particular we looked at the ratio of distance distributions for unlike and like pairs, and at the average closest separations. The results are presented in fig. 6 and table 3. We are mainly interested in small separations, R , as we would expect there to be no observable difference for well-separated objects. As can be seen from table 3, we

find that unlike pairs are closer than like pairs. The decrease in R with correlation length is understandable as the larger g^2 corresponds to a larger physical volume, and hence a larger number of objects within that volume. In fig. 6 we plot $dN(U)/dN(L)$, the ratio of distributions of unlike to like pairs, and find that at small separations, this ratio is greater than one, indicating that there are indeed more unlike pairs at smaller distances. At *very* small distances any possible signal is destroyed by the cooling process, and at large separations there would seem to be as many like as unlike pairs, as intuition would suggest. We found that the number of like and unlike pairs were consistent across all coolings and the three values of g^2 we used. This is clearly an area of some interest in which more work than our preliminary study could be undertaken.

g^2	Separation	R	# discounted	# used
0.8	I-I	4.371(62)	73	927
	A-A	4.426(64)	72	928
	I-A	3.331(33)	21	979
	U/L	0.757(18)		
0.84	I-I	3.914(54)	7	993
	A-A	3.828(57)	8	992
	I-A	2.781(24)	0	1000
	U/L	0.718(16)		
1.00	I-I	2.681(26)	0	1000
	A-A	2.612(27)	0	1000
	I-A	2.090(16)	0	1000
	U/L	0.789(14)		

Table 3: The closest separation of objects at the different values of g^2 under differing amounts of cooling. The entries denoted ‘U/L’ are the ratios of the I-A separations to the average of the I-I and A-A. The 4th and 5th columns are, respectively, the number of configurations for which a calculation was not possible (ie those containing only one or fewer (anti-)instantons) and the number of configurations used in the actual measurement.

We compare our method of analysis of the large scale topological objects with that used by other workers. In [18] the size of $SU(2)$ instantons was estimated by calculating the topological charge density correlation function

$$f(x) = \sum_y Q(y)Q(x+y) \quad (20)$$

with the sum over the whole lattice. Then $f(x)$ is fitted for each instanton at a particular value of ρ using a convolution of an analytic continuum expression

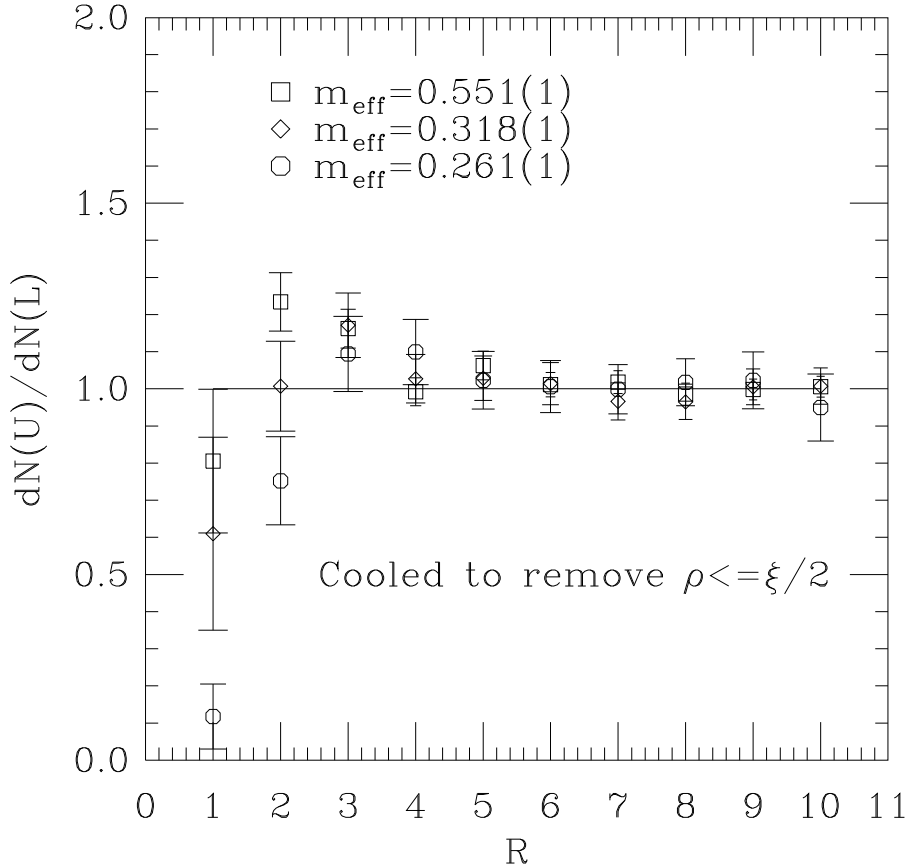


Figure 6: The ratio of separation distributions between pairs of unlike and of like objects, calculated on configurations cooled to remove $\rho \lesssim \xi/2$.

similar to eq. 13:

$$Q_\rho(x) = \frac{6}{\pi^2 \rho^4} \left(\frac{\rho^2}{x^2 + \rho^2} \right)^4 \quad (21)$$

Elsewhere, in [19], $SU(2)$ instanton size data are obtained from two methods: first a simple extraction of a size from the continuum single-instanton relation

$$S_{max} = \frac{48}{g^2} \frac{1}{\rho^4} \quad (22)$$

and a second method which measured the extent of the instanton only in the lattice axis directions, and then took the average of these numbers as the size.

Different methods can give different results, particularly for $O(3)$, since the vacuum is not well approximated by a dilute gas of instantons. We believe that our method of assigning “instantons” is more robust and works well even if the instantons are not well-separated. Our method works for moderately cooled configurations and does not rely upon the configurations having been cooled to such

an extent that they are no longer representative of the pre-cooled physics. Furthermore, the methods used in [19] rely explicitly on the instantons having a circular geometry, just as those generated by eq. 9 do; it is clear from fig. 2, and from the results shown in [3], that, in $O(3)$ at least, artificially generated isolated instantons are not representative of those obtained from a simulation of the vacuum.

5 Conclusions

In this paper we have extended the work begun in [3], and shown that it is possible to obtain a distribution of large size topological objects that is, within some size range, independent of the cooling performed. We have put forward the criterion for an optimum cooling to be such that objects of size $\mathcal{O}(2a)$, ie twice the lattice spacing be removed by the cooling process. At our values of g^2 , this corresponds to objects with size of the order of half the correlation length be removed. Furthermore, we find results that can be interpreted as applicable to the continuum distribution, as they are independent over a range of lattice spacing varying by a factor of two.

We confirm, by non-perturbative study, that the distribution of size of topological objects is peaked at small size. Roughly our results are that

$$\frac{1}{V} \frac{dN}{d\rho} \sim \frac{1}{\rho^3} \quad (23)$$

(with $N = S/S_I$). This contrasts with the inverse size distribution expected for a dilute gas of instantons.

We have also shown, in figs. 2 and 3, that the dilute instanton gas is not a good model for the $O(3)$ vacuum at the values of g^2 we used, and made a preliminary study of the relative distributions of instanton and anti-instanton separations, and found them to be correlated to the extent that unlike pairs exist at smaller separations than like pairs of objects.

Appendix A Instantons on a torus

In this appendix we present an argument that it is not possible to place a single instanton on a torus.

If we write the action and topological charge in terms of $\omega, \bar{\omega}$ we get [20]:

$$S(\omega) = \frac{4}{g^2} \int \frac{d^2x}{(1 + \omega\bar{\omega})} (\partial_z \omega \partial_{\bar{z}} \bar{\omega} + \partial_z \bar{\omega} \partial_{\bar{z}} \omega) \quad (24)$$

and

$$Q(\omega) = \frac{1}{\pi} \int \frac{d^2x}{(1 + \omega\bar{\omega})} (\partial_z \omega \partial_{\bar{z}} \bar{\omega} - \partial_z \bar{\omega} \partial_{\bar{z}} \omega) \quad (25)$$

which lead us to the following expression for S :

$$S(\omega) = \frac{4\pi}{g^2} |Q(\omega)| + \frac{8}{g^2} \int \frac{d^2x}{(1 + \omega\bar{\omega})} |\partial_{\bar{z}}\omega|^2 \quad (26)$$

Instantons are locally stable, finite-action solutions to the Euclidean equations of motion, and as such are given by

$$\partial_{\bar{z}}\omega = 0 \quad (27)$$

and we therefore require ω to be an analytic function.

If we now take a rectangular region, R , of \mathbb{R}^2 and impose toroidal boundary conditions, then (∂R denoting the boundary of R)

$$\oint_{\partial R} \omega(z) dz = 0 \quad (28)$$

as there is a pairwise cancellation of the line integral along opposite sides of R . Cauchy's theorem then implies that

$$\sum \text{residues} = 0 \quad (29)$$

and thus that one cannot have a single-instanton solution to the equations of motion on a torus (as its residue would be identically zero) but multi-instanton solutions are possible. As shown in [20], a periodic solution of eq. 27 on R can be expressed in terms of the Weierstrass σ function.

References

- [1] M. Lüscher, Nuc. Phys. **B200**, 61 (1982).
- [2] P. Hasenfratz, P. Maggiore, F. Niedermayer, Phys. Lett. **B265**, 522 (1990)
- [3] *Topography of the cooled $O(3)$ vacuum*, P.S. Spencer and C. Michael, Liverpool preprint LTH 328, hep-lat/9401011. Holland (1982).
- [4] A. Di Giacomo et al, *Topological Susceptibility on the Lattice: the 2d $O(3)$ Sigma Model*, CERN preprint TH-6382/92.
- [5] H. Arisue, Phys. Lett. **140B**, 383 (1984).
- [6] *Instantons from over-improved cooling*, Margarita Garcia Perez, Antonio Gonzalez-Arroyo, Jeroen Snippe and Pierre van Baal, preprint INLO-PUB-11/93, FTUAM-93/31.
- [7] *Perfect Lattice Action For Asymptotically Free Theories* P. Hasenfratz and F. Niedermayer, BUTP-93/17.

- [8] A. Di Giacomo, E. Vicari, Phys. Lett. **275B**, 429 (1992).
- [9] B. Berg, M. Lüscher, Nucl. Phys. **B190**, 365 (1981).
- [10] B. Berg, Phys. Lett. **104B**, 475 (1981).
- [11] M. Camprostrini et al, *Topological susceptibility and string tension in the lattice CP^{N-1} models*, Pisa preprint IFUP-TH 34/92.
- [12] E. Mottola & A. Wipf, Phys. Rev. D **39**, 588 (1989).
- [13] *Gauge Fields and Strings* A.M. Polyakov, North
- [14] A.P. Bukhvostov, L.N. Lipatov, Nucl. Phys. **B180**, 116 (1981).
- [15] S. Coleman, *The Uses of Instantons*, lectures given at *Ettore Majorana*, 1977.
- [16] *Solitons and Instantons*, Rajaraman, North Holland.
- [17] V.A. Novikov et al, Phys. Lett. **139B**, 389 (1984).
- [18] M.-C. Chu, J.M. Grandy, S. Huang, J.W. Negele, *Evidence for the Role of Instantons in Hadron Structure from Lattice QCD*, to appear in Proceedings of LATTICE '93 (Dallas), MIT-CTP-2260.
- [19] M.I. Polikarpov, A.I. Veselov, Nucl. Phys. **B297**, 34 (1988).
- [20] J.L. Richard, A. Rouet, Nucl. Phys. **B211**, 447 (1983).